Femtosecond laser damage threshold and nonlinear characterization in bulk transparent SiC materials

G. Logan DesAutels,[1] Chris Brewer,[2] Mark Walker,[4] Shane Juhl,[2] Marc Finet,[1] Scott Ristich,[1] Matt Whitaker,[1] and Peter Powers[3]

[1]*AT&T Government Solutions, Dayton, Ohio 45433 USA*
[2]*Air Force Research Laboratory, Materials and Manufacturing Directorate, Wright-Patterson Air Force Base, Ohio 45433 USA*
[3]*University of Dayton, Dayton, Ohio 45469 USA*
[4]*General Dynamics Information Tech, Dayton, Ohio 45431 USA*

Received September 10, 2007; revised October 15, 2007; accepted October 18, 2007; posted November 7, 2007 (Doc. ID 87344); published December 21, 2007

Semi-insulating and conducting SiC crystalline transparent substrates were studied after being processed by femtosecond (fs) laser radiation (780 nm at 160 fs). *Z*-scan and damage threshold experiments were performed on both SiC bulk materials to determine each sample's nonlinear and threshold parameters. "Damage" in this text refers to an index of refraction modification as observed visually under an optical microscope. In addition, a study was performed to understand the damage threshold as a function of numerical aperture. Presented here for the first time, to the best of our knowledge, are the damage threshold, nonlinear index of refraction, and nonlinear absorption measured values. © 2007 Optical Society of America

OCIS codes: 190.0190, 190.4180, 190.5970.

1. INTRODUCTION

Femtosecond (fs) lasers have become a very important tool for micromachining and fabrication of photonic devices. Their unique ability of inducing permanent index changes into just about any transparent material is due to fast focusing conditions, resulting in very high intensity and causing nonlinear multiphoton absorption. Former research has theorized that the ultrafast pulse is too short to interact at the molecular level and instead interact at the atomic electronic level [1]. Here the fs pulse displaces electrons permanently and/or causes lattice changes, resulting in a modification to the index of refraction [2]. The modification to the index is localized to a very small volume, depending on the NA and energy used. These index alterations can be on the surface or, in most cases, subsurface to the bulk material.

SiC is an attractive alternative material for a variety of semiconductor devices where silicon (Si) lacks the environmental resistance that carbon furnishes when combined to Si [3]. These areas where SiC devices can be used include high-power high-voltage switching applications, high-temperature electronics, and avionics where it is desired to keep sensitive Si-based electronics away from extreme environments onboard aircraft [3]. However, micromachining SiC is problematic owing to its ability to resist almost any type of etching process. Examples of common etching processes are wet chemical etching, deep reactive ion etching, and reactive ion etching [4]. For these reasons, it is of some interest to study the laser processing and material characteristics of SiC to provide future alternative methods of micromachining this unique material.

Our method of morphing a circular beam into a high-aspect-ratio elliptical beam uses an anamorphic lens. The anamorphic lens provides accurate micromachined lines in the absence of any self-focusing from the use of a highly elliptical beam [5]. The idea or theory is that a large numerical aperture (NA) in combination with an elliptical beam will decrease the chances of any self-focusing occurring within the bulk of the sample. Self-focusing filamentation will spoil the micromachined features, which will result in unpredictable or undesired micromachined features. The gratings produced with the anamorphic lens resist any nonlinear self-focusing attributes and result in clean, accurate gratings that closely resemble the geometrical profile.

The anamorphic lens transforms the ultrafast laser pulse from a 5.5 mm round Gaussian fluence distribution to a 2.5 μm by 190 μm line shape. The SiC samples were laser processed using an automated *xyz* stage in a direct-write configuration. The samples were irradiated with a single laser pulse by use of a chopper wheel and high-speed shutter combination. The fs laser pulse was generated using a Clark-MXR CPA-2010 laser system with a wavelength of 780 nm, a pulse width of 150–200 fs, $M^2=1.55$, and a maximum energy of 1 mJ/pulse. Typical pulse energies used in this work were in the 10–30 μJ range.

In this work we report semi-insulating and conducting SiC bulk material linear and nonlinear optical properties as well as bulk damage threshold (DT) measurements as a function of NA (under tight focusing conditions). The linear SiC material properties were measured using a UV–Vis spectrometer that determines the linear trans-

 © 2008 Optical Society of America

mission and bandgap of the substrate. The third order nonlinear properties are revealed using the Z-scan technique, which presents the nonlinear absorption (β) and the nonlinear index of refraction (n_2). The laser-processed portions of the samples were also investigated using optical microscope imagery and atomic force microscopy (AFM). Finally, all experiments were first calibrated using a fused silica (FS) sample and compared to referenced experimental data to validate our results.

2. EXPERIMENTAL SETUPS

The DT and Z-scan experiments were completed using a single laser source split into multiple paths. Figure 1 illustrates the experimental setups.

Figure 1 gives the experimental setups for both the DT and Z-scan experiments. The Clark-MXR fs laser system is split into multiple beam paths for different tests; a 100 μJ portion of that is split for the DT and Z-scan studies. In each experiment line there is a polarizer beam splitter and half-wave-plate combo used to attenuate the beams. The Z scan uses a 750 mm lens to provide a large Rayleigh range Z_R to keep the fluence below the damage threshold. The DT experiment uses the anamorphic lens to morph the 5.5 mm circular beam into a 2.5×190 μm line distribution as described in Section 1.

The Z-scan line uses a CCD camera (DALSA 1M15) to sense the transmitted beam, and the closed aperture is added synthetically via software image processing. The synthetic aperture types (round or other shapes), the range of the Z scan, and the camera calibration are all set before each scan. The experiment uses a large CCD array (typically about twice the beam diameter after focus), and synthetic apertures have allowed ease in alignment of the beam down the Z-scan line. In addition, the software can record an average of beam profiles (intensity) at each Z location and then save those images for further analyses.

The DT line uses input and output photodiodes to measure the incident pulse energy versus the transmitted energy through the sample. Each photodiode is calibrated using a pyroelectric joule meter traceable to the National Institute of Standards and Technology (NIST). The DT line also has a chopper wheel and a high-speed shutter that together work automatically to control the number of pulses to the sample. Finally, the sample is held on an xyz automatic stage controlled with ±1 μm accuracy. The entire illumination collection procedure is automated. This configuration, shown in Fig. 1, allows for the Z scan and DT experiments to run simultaneously, but the beams delivered at each experiment are separately characterized for completeness.

3. SiC CHARACTERISTICS

The SiC samples tested are two types shown in Table 1 below.

Each sample in Table 1 was perpendicularly oriented on the c plane with the vertically polarized circular and anamorphic beams. The nitrogen dopant amounts ($\sim$1 part per million) in the conducting sample are so small that they can be ignored for this study. The thickness differences between the samples can also be ignored, since these are surface studies. The lab and laser conditions are identical. Once the lenses were aligned and characterized, each sample was simply inserted at the same location. Because the samples have the same dimensions, the identical sample mount/position was employed. The tests were run back-to-back, so the laboratory environmental conditions were indistinguishable. Thus, the conductivity/resistivity is the only variable between the two samples.

4. THRESHOLD MEASUREMENTS

The damage threshold in this paper refers to substrate modification observed under an optical microscope using transmission or reflection. The DT values are an important quantity to report for future laser processing of SiC bulk materials. The DT is measured in joules per square centimeter for a low NA and a high NA and determines the minimum energy distribution to induce an observable change into the SiC material. The fluence distribution in the beam focus is well designed as an elliptical and/or circular Gaussian, with spot size along each principal axis given by [6]

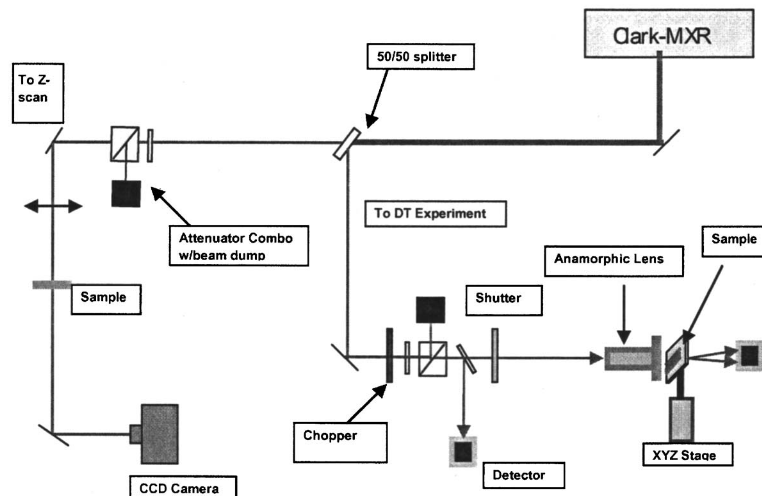

Fig. 1. Optical setup for damage threshold and Z-scan experiments.

Table 1. SiC Sample Characteristics for Semi-insulating and Conducting Types[a]

Sample	Orientation	Dopant	Dopant Concentration (cm^{-3})	Resistivity (O·cm)	Thickness (μm)	Face	N or P Type
SiC semi-insulating	*c*-plane, 6H 0° on axis	Undoped	$\sim 1\times 10^{15}$	3×10^{7}	340	Si	—
SiC conducting	*c*-plane, 6H 0° on axis	Nitrogen	$\sim 2.5\times 10^{17}$	0.05	220	Si	N

[a]Semi-insulating SiC samples are supplied by Intrinsic Corp, and conducting SiC samples are supplied by Cree Corp.

$$w_{ox,y} = \frac{\lambda f_{x,y} M^2_{x,v}}{\pi w_z}, \quad (1)$$

where f is the focal length, λ is the wavelength, M^2 is a measured quantity that is used to characterize the deviation from diffraction limited focusing (M^2 of 1 represents the diffraction limit, and real beams have $M^2 > 1$), and w_z is the spot radius propagating from the laser and is given as

$$w_z = w_{ox,y}\sqrt{1 + \left(\frac{Z}{Z_R}\right)^2}, \quad (2)$$

where Z is the propagation distance from the laser source to the test bed, w_o is the beam spot size, and Z_R is the Rayleigh range. The peak fluence can be determined using

$$F_o = \frac{2E}{\pi w_{ox} w_{oy}}, \quad (3)$$

where E is the input energy. The above equations were used for each axis for the elliptical beam formed by the anamorphic lens system, which produced a high NA beam. Figure 2 and Table 2 then give the damage threshold results for FS, semi-insulating and conducting SiC.

These DT results greatly depend on NA as shown in Schaffer–Mazur [5] for tight focusing conditions. In the top chart in Fig. 2, the low NA DT data was recorded using a 125 mm lens (NA=0.022). To show the dependence of NA, as Schaffer–Mazur, we employed our anamorphic lens and repeated the high NA (0.256 in the y direction) DT plot shown in the bottom chart in Fig. 2. Each DT experiment was done using 780 nm at 160 fs. The low and high NA DT results are tabulated in Table 2 below.

As shown in Table 2, the use of a high NA focusing geometry increases the DT, as inspected under an optical microscope, by a factor of 6 to 10 times from the spherical 125 mm lens. The FS sample did not reach a DT for the high NA experiment, and it is predicted that 100 μJ (for a fluence of $\sim$30 J/cm^2) or more is needed to create a 2.5 μm $\times$ 190 μm line on or below the surface.

5. Z-SCAN STUDY

The nonlinear properties, nonlinear index of refraction (n_2), and nonlinear absorption (β) of SiC semi-insulating and SiC conducting were also investigated. In calculating the nonlinear parameters, two approximations are applied to reduce the computation speed and complexity. One is a thin sample approximation where the sample thickness $\gg Z_R$, and the second is the weak nonlinear approximation that assumes the nonlinear process is small [11]. The calculated n_2 data is done using the peak to valley of the closed aperture trend defined by [12]

$$n_2 = \frac{\Delta\Phi_o}{kL}\frac{1}{I_o}, \quad (4)$$

where $\Delta\Phi_0$ is the on-axis phase shift at the focus, k is the wave number, L is the length of the sample and $I(z,E)$ is the intensity as a function of the z position and energy for a secant pulse given by [12]

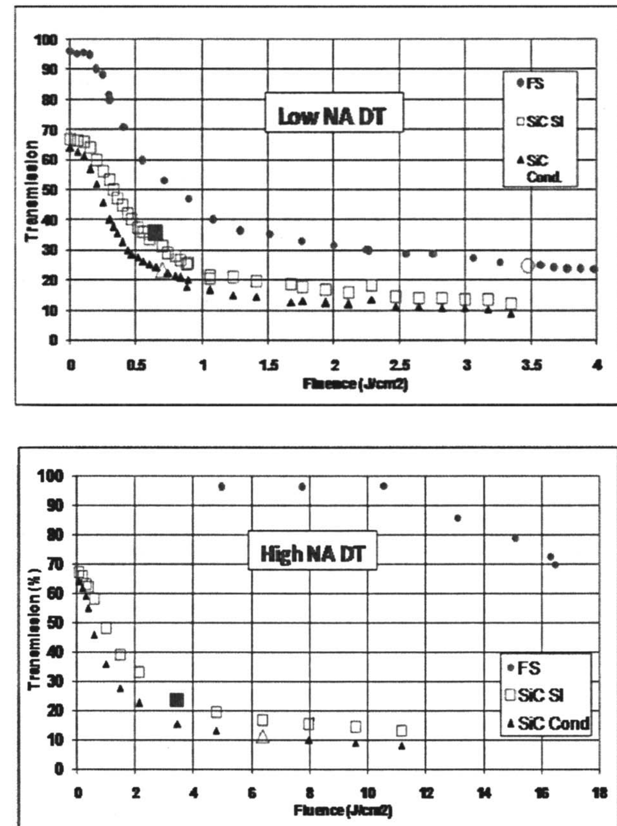

Fig. 2. Top, a plot of DT for SiC SI, SiC conducting, and FS using a spherical 125 mm lens (NA=0.022) for 780 nm at 160 fs. FS is baseline sample used to calibrate our DT experiments. FS has a DT that is well known to be $\sim$3.0–4.0 J/cm^2 as referenced [7]. Bottom, the high NA DT plot of SiC semi-insulating, SiC conducting, and FS using an anamorphic lens (NAx=0.0035 in x and NAy=0.256 in y) for 780 nm at 160 fs. The large solid squares and open triangles represent where the visible damage begins.

Table 2. DT Measured Results for Two Lenses, 125 mm Focal and Anamorphic Lens (High NA), Using 780 nm at 160 fs

Sample	Low NA DT (J/cm^2)	High NA DT (J/cm^2)	Bandgap (eV)
FS	3.7	~20 to 40	90 [8]
SiC semi-insulating	0.6	3.5	3.14 [9,10] and figure
SiC conducting	0.65	6.4	3.14 [9,10] and figure

$$I(z,E) = \frac{2E\ln(1+\sqrt{2})}{\Delta t \pi w_o^2}, \quad (5)$$

where Δt is the pulse width, and w_x and w_y are the spot radii of the beam in the x and y directions. As stated above, $\Delta\Phi_o$ is the on-axis phase shift $\Delta\Phi$, which can be experimentally determined by examining the peak–valley transmission change in the closed aperture case using [12]

$$|\Delta\Phi_o| = \frac{\Delta T_{pv}}{(0.406)(1-S)^{0.25}}, \quad (6)$$

where S is the linear transmittance aperture (S parameter) and is defined by [12]

$$S = 1 - \exp\left(-2\frac{r_a^2}{w_a^2}\right). \quad (7)$$

Here, r_a is the radius of the closed aperture and w_a is the radius of the laser beam at the location of the closed aperture. Equation (4) can then be used to recover the n_2 value of the sample under test.

To simplify this paper, we will not go into much detail with the fit data; rather, we direct the reader to [13], which describes precisely how to apply the theory and equations to any mathematical software such as Mathcad, Matlab, etc. The normalized open aperture signal is fitted to [13]

$$Tx(z,\beta,E) := \frac{1}{2q_o(z,\beta,E)}\int_{-\infty}^{\infty} \ln(1+q_o(z,\beta,E)\mathrm{sech}(x)^2)\mathrm{d}x, \quad (8)$$

where q_o is defined by [13]

$$q_o(z,\beta,E) := \beta I(z,E)L. \quad (9)$$

This work utilizes the open and closed fits to average the noise in the data. The peak–valley of the closed data fit is used to calculate the on-axis phase shift.

For the FS and SiC data, we used a synthetic closed aperture of 0.55 mm, an open aperture of 5 mm, a repetition rate of 41 Hz (with assistance from a chopper wheel), an S parameter set to 15%, and energy ranging from 2 to 4 μJ. Multiple energies were used to ensure consistent nonlinear measurements. The beam was characterized before the experiments by performing an M^2 measurement, the pulse width using a Clark-MXR AC 150 autocorrelator, and profiling the beam with a Cohu CCD camera. The beam was profiled with and without the sample to properly calculate the S parameter [shown in Eq. (7)]. Representative Z-scan data is shown as raw data with open and closed aperture data fits, which provide the n_2 and β results. The results for the SiC and FS Z scans are found in Table 3.

From Table 3, the semi-insulating and conducting SiC nonlinear properties are relativity the same, which is not surprising, since the dopant levels in the conducting sample are extremely small, as stated earlier. The conductivity is electronic, therefore it has no or little effect on the optical linear/nonlinear interactions, and thus the nonlinear quantities are about the same. The SiC β and n_2 experimental results were compared to a simple two-parabolic-band model by Sheik-Bahae *et al.*[14] for theoretically calculating the nonlinear absorption and index of refraction properties in semiconductors. The bandgap used to calculate the theoretical β and n_2 was calculated using the wavelength at the 1% transmission point in the UV–Vis chart in Fig. 3. This model was not used for FS, since it is not a semiconductor.

The FS data results show a β=0 cm/GW and n_2=2.6 $\times 10^{-7}$ cm^2/GW. Referenced FS Z-scan results show similar n_2 values of 2.5×10^{-7} cm^2/GW [15], but published β values were not located primarily owing to the fact that FS has little or no nonlinear absorption from its large bandgap. Since the FS n_2 experimental result is in good agreement with the published values, the Z-scan experiment is in good working order and is ready to test the SiC samples. The SiC samples were tested, and the results are given in Fig. 4.

6. UV–VIS STUDY

A UV–Vis study was carried out to understand the linear transmission and to confirm the provided bandgap information shown in Table 2 using a Varian Cary 50 UV–Vis spectrometer. This device uses a xenon flash lamp and monochromatic optics to send a beam of varying wavelengths (300 to 900 nm) through the sample to measure its transmission. The results for each SiC sample are given in Fig. 4.

Table 3. Nonlinear Measurements Resulting from *Z*-scan Experiment Using 780 nm at 160 fs[a]

Sample	β (cm/GW) Theory	β (cm/GW) Measured	n_2 (cm^2/GW) Theory	n_2 (cm^2/GW) Measured
FS	NA	0	NA	2.60×10^{-7}
SiC semi-insulating	0.055	0.064	3.6×10^{-6}	4.75×10^{-6}
SiC conducting	0.055	0.052	3.6×10^{-6}	4.00×10^{-6}

[a]Multiple energies were tested to provide a statistical average.

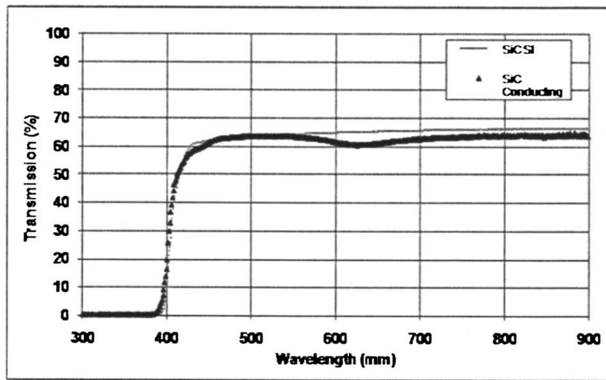

Fig. 3. UV–Vis results on semi-insulating and conducting SiC.

From the Uv–Vis results, it demonstrates that both the semi-insulating and conducting SiC samples have a band edge at 400 nm. Equation (10) relates the cutoff wavelength of the SiC samples to the band gap in electron volts (cV):

$$\lambda = \frac{1239.8}{E(eV)}. \tag{10}$$

Here, E is the energy with units of electron volts, λ is in units in nanometers, and Table 2 gives $E = 3.1$ eV. Therefore, $\lambda = 399.936$ nm for both semi-insulating and conducting SiC, which is in agreement with the turn-on wavelength in Fig. 3. Furthermore, the conducting SiC sample has a dip centered at ~ 630 nm that is consistent with multiple SiC conducting samples tested. The dip may be due to the absorption of the nitrogen dopant present in the conducting SiC sample. The transmissions are around 65–70% for each semi-insulating and conducting sample, which agrees with the DT results that show a nonlinear transmission at close to zero fluence.

7. SAMPLE CHARACTERIZATION

The high NA line distribution processed into the SiC semi-insulating and conducting samples were further analyzed using optical microscopy and AFM to understand the morphology of the index-modified structures. The processed lines are on or just below the surface (~ 5 to $10\ \mu$m), and the modifications form a hill–valley above and below the surface, depending on the type of SiC processed. Figure 5 below illustrates this effect. For these images, the optical microscope used is an Olympus upright digital BX51 microscope with Nomarski DIC capabilities that uses high contrast prisms to produce increased contrast and resolution. This microscope also has measuring capabilities to $\pm 0.25\ \mu$m or less, which is also traceable to NIST.

Here, the $2.5\ \mu\text{m} \times 190\ \mu$m predicted line spread is shown from the AFM to be $\sim 5.5\ \mu$m wide $\times 210\ \mu$m long for the semi-insulating SiC and $\sim 3.3\ \mu$m wide $\times 193\ \mu$m long for the conducting SiC sample. The difference in the predicted result primarily comes from the sample makeup and the sample being at the exact focus as foreseen. The line spread (for both semi-insulating and conducting) decreases in both axes as the fluence or energy is decreased to the point where no visible damage occurs. The semi-insulating SiC sample results in more columns of modified lines, which are due to its having a lower threshold than the conducting SiC sample. The processed lines on both SiC types were analyzed using the Nomarski DIC mode on the optical microscope set in reflection mode. The semi-insulating SiC processed lines are more optically opaque, which may be caused by bulges or hills that form in the surface as observed in other types of bulk transparent dielectric substrates. AFM imaging will give a more precise measurement of the line spread morphology.

AFM was performed using a Veeco Dimension 3100 with a Nanoscope 3a controller in tapping mode to evaluate the topography of line distributions fabricated just above the threshold. The height images were obtained from monitoring the cantilever oscillation amplitude during scanning. Figure 6 below shows some AFM results of a SiC semi-insulating sample with surface line modifications.

The AFM results show a morphology of the line processed structures as being 3–5 μm in width and about a 10–30 nm hill or valley. The semi-insulating SiC sample forms line-protruding bulges that are raised by ~ 10 nm and have a width of $\sim 5.5\ \mu$m. The conducting SiC sample forms line trenches that are ~ 30 nm deep and have a width of $\sim 3.3\ \mu$m. The AFM concludes that the semi-insulating SiC surface modification by these line spreads creates a hill in the substrate surface, which may be because a local subsurface restructuring has occurred, or some other electronic trapping process [16] has forced the material to rise in the processed areas. On the contrary,

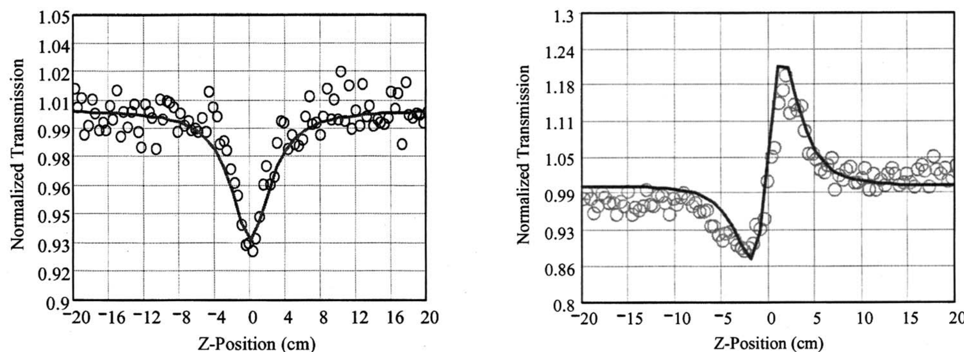

Fig. 4. Left, the normalized transmission for the open aperture; right, the normalized transmission for the closed aperture, both for the SiC semi-insulating sample. The parameters used for this sample were energy of 3 μJ, a 750 mm lens, a wavelength of 780 nm, a pulse width of 160 fs, and a 5.1 mm entrance aperture.

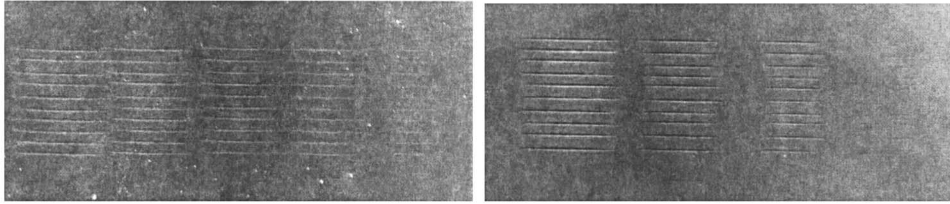

Fig. 5. DT optical microscope results using Nomarski DIC and image processing for better viewing purposes for (left) semi-insulating SiC and (right) conducting SiC. Image processing was performed to better resolve modified surface lines. These results were both done using 780 nm at 160 fs.

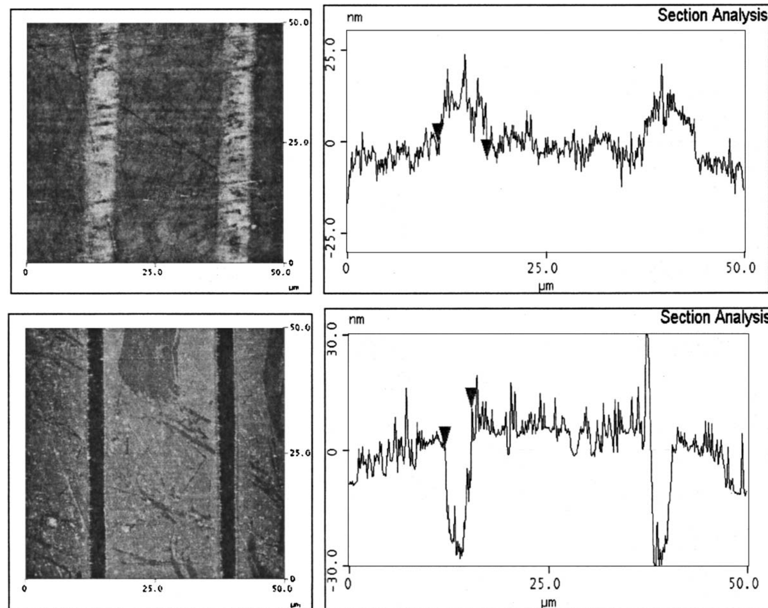

Fig. 6. Top, AFM results of a 5.5 μm wide and a 10 nm raised surface modification on semi-insulating SiC material. Bottom, conducting SiC sample AFM results of a 3.3 μm wide and a 30 nm trench surface modification.

the conducting SiC sample forms trenches that may be due to surface structural damage caused by thermal breakdown of the molecular lattice, to the inability for the crystal to dissipate heat, and/or to oxidation and chemical reactions on the surface that give a different compound. The protruding lines in the semi-insulating sample also caused a broader linewidth instead of the predicted 2.5–3 μm, and the valleys formed in the conducting samples create a sharper edge that results in a closer agreement with the predicted value. In any case, there is a morphology difference in the femtosecond laser processing of SiC between semi-insulating and conducting types. X-ray diffraction was performed on these SiC samples, but it was found that the damage areas were too small for the x-ray beam and only the bulk SiC was actually being measured—thus the x-ray diffraction tests were unsuccessful.

8. CONCLUSION

In this work we report important linear, nonlinear, and femtosecond laser processing threshold properties that are useful to optical and material scientific communities. We concluded that there are only two observable differences between the two SiC types (even the samples' visual appearance is similar), which are the UV–Vis absorption at ~630 nm and the morphology after being fs laser processed. The linear, nonlinear, and DT properties remain familiar to one another. The values of all the measured parameters vary within 20% of each other except for the high NA DT values, which gives a 45% difference between semi-insulating and conducting types.

ACKNOWLEDGMENTS

Special thanks is given to Air Force Research Laboratory personnel Don Dorsey and Tom Kensky for providing the SiC samples, Bill Mitchell for providing information on each of the SiC samples, William Woody for help with the image processing, and Angela Campbell for assisting with AFM results.

REFERENCES

1. G. Petite, P. Daguzan, S. Guizard, and P. Martin, "Femtosecond history of free carriers in the conduction band of a wide-bandgap oxide," in IEEE Annual Report Conference on Electrical Insulation and Dielectric Phenomena (IEEE, 1995), Vol. 15, pp. 40–44.
2. A. Tien, S. Backus, H. Kapteyn, M. Murnane, and G. Mourou, "Short-pulse laser damage in transparent materials as a function of pulse duration," Phys. Rev. Lett. **82**, 3883–3886 (1999).
3. J. Copper, Purdue Wide Band Gap Semiconductor Device Research Program, Purdue University College of Engineering, http://www.ecn.purdue.edu/WBG/Index.html.

4. Y. Dong and P. Molian, "Femtosecond pulsed laser ablation of 3C-SiC thin film on silicon," Appl. Phys. A **77**, 839–846 (2003).
5. J. Ashcom, C. Schaffer, and E. Mazur, "Numerical aperture dependence of damage and supercontinuum generation from femtosecond laser pulses in bulk fused silica," J. Opt. Soc. Am. B **23**, 2317–2322 (2006).
6. J. Verdeyen, *Laser Electronics*, 3rd ed. (Prentice Hall, 1995), pp. 50–55.
7. M. Lenzner, J. Kruger, S. Sartania, Z. Cheng, Ch. Spielmann, G. Mourou, W. Kautek, and F. Krausz, "Femtosecond optical breakdown in dielectrics," Phys. Rev. Lett. **80**, 4076–4079 (1998).
8. A. M. Strelstov, J. K. Ranka, and A. L. Geata, "Femtosecond ultraviolet autocorrelation measurements based on two-photon conductivity in fused silica," Opt. Lett. **23**, 798–800 (1998).
9. L. Shah, J. Tawney, M. Richardson, and K. Richardson, "Self-focusing during femtosecond micromachining of silicate glasses," IEEE J. Quantum Electron. **40**, 57–68 (2004).
10. A. Evwaraye, S. Smith, and W. Mitchel, "Persistent photoconductance in in n-type 6H-SiC," J. Appl. Phys. **77**, 4477–4481 (1995).
11. P. Chapple, J. Staromlynka, J. Herman, T. McKay, and R. McDuff, "Single-beam Z-scan: measurement techniques and analysis," J. Nonlinear Opt. Phys. Mater. **6**, 251–293 (1997).
12. M. Sheik-Bahae, A. Said, T. Wei, D. Hagan, and E. van Stryland, "Sensitive measurement of optical nonlinearities using a single beam," IEEE J. Quantum Electron. **26**, 760–769 (1990).
13. M. Yin, H. P. Li, S. H. Tang, and W. Ji, "Determination of nonlinear absorption and refraction by single Z-scan method," Appl. Phys. B **70**, 587–591 (2000).
14. M. Sheik-Bahae, D. Hutchings, D. Hagan, and E. van Stryland, "Dispersion of bound electronic nonlinear refraction in solids," IEEE J. Quantum Electron. **2**, 1296–1309 (1991).
15. M. Yamane and Y. Asahara, *Glasses for Photonics* (Cambridge U. Press, 2000), p. 174.
16. S. Mao, F. Quére, S. Guizard, X. Mao, R. Russo, G. Petite, and P. Martin, "Dynamics of femtosecond laser interactions with dielectrics," Appl. Phys. A **79**, 1695–1709 (2004).